Chemical Physics Letters 565 (2013) 132–137

Contents lists available at SciVerse ScienceDirect

Chemical Physics Letters

journal homepage: www.elsevier.com/locate/cplett

Mid-infrared continuous wave cavity ring-down spectroscopy of a pulsed hydrocarbon plasma

Dongfeng Zhao *, Joseph Guss, Anton J. Walsh, Harold Linnartz

Raymond and Beverly Sackler Laboratory for Astrophysics, Leiden Observatory, University of Leiden, P.O. Box 9513, NL 2300 RA Leiden, The Netherlands

ARTICLE INFO

Article history:
Received 7 December 2012
In final form 5 February 2013
Available online 21 February 2013

ABSTRACT

We describe an ultra-sensitive method to record high-resolution mid-IR spectra of hydrocarbon-chain species and other astrophysically relevant molecular transients in a pulsed planar plasma expansion. The method uses an all fiber-laser-based optical parametric oscillator (OPO) light source, in combination with continuous wave cavity ring-down spectroscopy (cw-CRDS) as a direct absorption detection tool. A hardware based multi-trigger concept is introduced to apply cw-CRDS to pulsed plasma. The performance and potential of the method are illustrated and discussed, based on extended and fully rotationally resolved sample spectra of HC_4H and HC_6H, generated in the discharge of an expanding C_2H_2/He/Ar gas mixture.

1. Introduction

Carbon chains and their derivatives, $X_mC_nY_l^{(+/-)}$, with X and Y typically H, N, O, or S, have attracted much interest because of their relevance to the chemistry of the interstellar medium (ISM). The spectroscopic characterization of these reactive species, both in the laboratory and in the ISM, from the microwave to the UV, has been the topic of many studies over the last few decades. Fourier transform laboratory microwave studies [1] have made possible the discovery of tens of highly unsaturated carbon-chain species [2], including linear $HC_{11}N$ [3], and ions such as $HCCCNH^+$ [4], C_6H^- [5], and C_8H^- [6]. For linear centro-symmetric chains, like the bare carbon species C_n [7–11] and polyacetylenes ($HC_{2n}H$) [12,13] – radio-silent due to the lack of a permanent dipole moment – mid- or far-infrared (IR) spectroscopy offers a powerful alternative approach for detection and characterization. Since carbon-chain species are considered to be potential carriers of the diffuse interstellar bands (DIBs), i.e., optical absorption features observed in star light crossing translucent interstellar clouds [14,15], electronic spectra of carbon-chain species have also been studied extensively in the laboratory (see Refs. [11,16,17] for a review).

The present letter focuses on the laboratory detection of hydrocarbon-chain species in the mid-IR, a spectroscopic range well known as a molecular fingerprint region. Fourier transform IR spectroscopy has been widely used to investigate the ro-vibrational spectra of gas-phase molecules with high resolution and broad coverage [18,19]. The ongoing improvements and upgrades of narrow-band mid-IR light sources, such as tunable diode lasers (TDLs), quantum cascade lasers (QCLs), continuous wave optical parametric oscillators (cw-OPOs) and difference frequency generation (DFG) devices, allow laser based IR spectroscopic techniques to achieve high detection sensitivity and molecule selectivity [20]. Recently, ultra-sensitive cavity enhanced mid-IR spectroscopic techniques, such as continuous-wave cavity ring-down spectroscopy (cw-CRDS) [21–24] and noise-immune cavity-enhanced optical heterodyne velocity modulation spectroscopy (NICE-OHVMS) [25,26] have been introduced and applied to the study of astrophysically relevant molecular ions.

To date, laboratory high-resolution IR spectra of gas-phase bare carbon (C_n) chains [9–11,27] and the linear C_3Si_2 species [28,29] have been studied with IR-laser absorption spectroscopy and laser ablation of carbon rods. For other carbon-chain derivatives, particularly highly unsaturated hydrocarbon-chain species ($C_nH_m^{(+/-)}$, typically with $n > 2$ and $m \leqslant n$), accurate gas-phase IR data are only available for di- and tri-acetylene (HC_4H and HC_6H) [30,31]. High-pressure pulsed planar plasma expansions, generated by specially designed multi-layer slit discharge nozzles [32,33], have proven to be successful in producing large abundances of highly reactive molecular transients, and have been employed in a series of electronic spectroscopic studies of hydrocarbon-chain radicals [16,17,34,35]. The work presented here describes a flexible OPO-based cw-CRDS spectrometer capable of recording high-resolution mid-IR spectra of molecular transients in a pulsed plasma, specifically hydrocarbon-chain species. A new boxcar gated integrator based trigger and timing scheme is introduced to apply cw-CRDS as a continuous technique to a pulsed plasma expansion. The performance of this method is illustrated with a substantial spectral extension of the available transitions in the C–H stretch region of the polyacetylenes HC_4H and HC_6H.

* Corresponding author. Fax: +31 715278475.
E-mail addresses: zhao@strw.leidenuniv.nl, d.zhao@vu.nl (D. Zhao).

0009-2614/$ - see front matter © 2013 Elsevier B.V. All rights reserved.
http://dx.doi.org/10.1016/j.cplett.2013.02.025

2. Experimental details

A schematic of the experimental setup is shown in Figure 1, consisting of a slit-jet discharge nozzle, a cw-CRDS detection scheme, and a trigger and data acquisition (DAQ) system.

2.1. Slit-jet discharge nozzle

The pulsed planar plasma is generated by discharging an acetylene/rare gas mixture in a multi-layer slit discharge nozzle and is used to produce carbon-chain species. Details of this pulsed plasma source have been described previously [32,33]; recent applications are described in Refs. [34–36]. A 1:1 helium–argon gas mixture is seeded with 0.5% C_2H_2 and is expanded through the 300 μm × 3 cm slit throat of the discharge nozzle into a vacuum chamber that is evacuated by a roots blower pump station with a total pumping capacity of 4800 m^3/h. A high voltage pulse (∼1.2 ms, and $V/I \sim -1200$ V/50 mA) is applied to the two electrodes of the discharge nozzle, and timed to coincide with the gas pulse (∼1.5 ms) controlled by a pulsed valve (General Valve, Series 9, 2 mm orifice) mounted on top of the nozzle body. With the backing pressure of the precursor gas mixture at ∼15 bar, the local pressure at the slit throat is ∼5–6 bar when the pulsed valve is on, which is suitable for producing long carbon chains and other complex transient species in the plasma. The typical stagnation pressure in the chamber during jet operation is ∼0.02 mbar.

2.2. OPO-based cw-CRDS

The narrowband mid-IR light source used is the idler output of a commercial single-frequency single-mode cw-OPO system (Aculight, Argos 2400-SF, Module B). The cw-OPO uses a periodically-poled lithium niobate (PPLN) crystal and is pumped with a total power of 10 W at 1.06 μm by a distributed feedback (DFB) fiber laser (NKT Photonics, Koheras Basik Y-10) amplified in a fiber amplifier (IPG Photonics, YAR-10K-1064-LP-SF). The idler wave of the OPO has an effective bandwidth of ∼1 MHz over 80 ms, and a total output power of ∼1.2 W. The idler wavelength covers roughly the 3100–4200 cm^{-1} (3.2–2.4 μm) region and is continuously tunable over ∼100 GHz by tuning the wavelength of the seed laser (DFB fiber laser). A precisely controlled voltage (0–200 V) is applied to the piezo-electric transducer (PZT) of the seed laser to guarantee fine, 'mode-hop-free' tuning of the OPO-idler wavelength. Coarse tuning is achieved by adjusting both the intracavity etalon angle and the position of the PPLN crystal in the cw-OPO system.

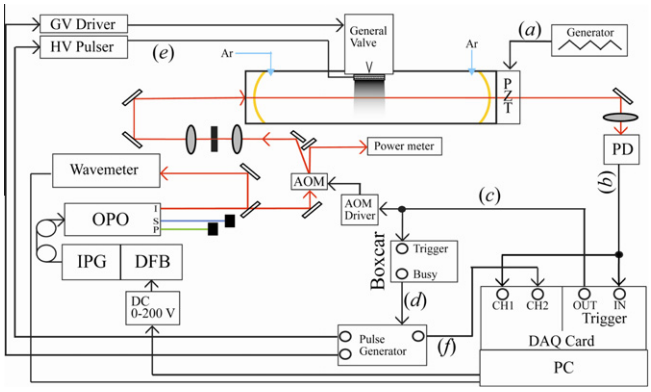

Figure 1. Schematic overview of the experimental setup. DFB: distributed feedback fiber laser (seeder); IPG: fiber amplifier; OPO: optical parametric oscillator with pump (P), signal (S) idler (I) beams; AOM: acousto-optic modulator; PZT: piezoelectric transducer; PD: photovoltaic detector. The time sequence of (a)–(f) is illustrated in Figure 2 and details are listed in the text.

The mode structure of the OPO idler output is mainly TEM_{00}, facilitating the use of cw-CRDS. The beam is directed through a germanium acousto-optic modulator (AOM). The first-order deflection, ∼10% of the idler wave under an angle of 15°, is spatially filtered by a two-lens telescope system configured with a 150 μm pinhole, and then coupled into the 56 cm long ring-down cavity. The cavity comprises two high reflectivity (R > 99.97% at 3 μm) plano-concave (1 m curvature) mirrors incorporated in high precision alignment tools that are mounted on opposite sites of an ISO-160 cross piece that also holds the plasma source. The optical axis of the ring-down cavity is parallel to, and ∼5 mm downstream from the slit throat of the discharge nozzle. Ring-down events are generated using a standard passive mode-locking scheme, as described in Refs. [21,37]. The cavity length is modulated at 20 Hz by applying a periodic triangle-wave voltage (trace a of Figure 2) to a PZT mounted on one of the mirror holders, ensuring that the cavity length is in resonance with the IR wavelength at least twice and at most four times in one period (trace b of Figure 2). This corresponds to a mirror translation of a little more than 1.5 μm. The cavity-transmitted light is detected by an IR-photovoltaic detector (Vigo System S.A., PVI-3TE-5, 50 MHz) and used as input to the signal and trigger channels of a fast DAQ card (Gage, Razor 1422, sampling rate 200 MS/s per channel). At the moment that the intensity of the cavity-transmitted light reaches a preset threshold value, the DAQ card is triggered and a synchronized TTL pulse from the trigger-out channel is generated (trace c of Figure 2). This TTL pulse is used to switch off the AOM, initiating a ring-down event that is quantified by its ring-down time (τ) using a fast exponential fitting algorithm [38]. Typical ring-down times in the present experiment amount to $\tau \sim 5$ μs.

2.3. Trigger and DAQ system

To apply cw-CRDS measurements to a pulsed plasma expansion, it is necessary to guarantee that the plasma pulse and the ring-down event coincide in time. To achieve this, several passive-mode-locking based detection methods have been successfully introduced in the past by a number of groups [22,33,39–41]. In general, these methods employ a programming-based multi-trigger and ring-down prediction scheme in the DAQ system. The latest variant of such DAQ software and software interfacing with pulse generators has been described in detail in the Supplementary material of Ref. [22].

In this work, we introduce a different concept, facilitating a hardware-based timing and trigger scheme. The detection principle is similar to that described in Refs. [22,39,41], but the implementation of a boxcar gated integrator (SRS, SR250) comes with a number of specific advantages. The trigger-out of the DAQ card (trace c of Figure 2) is not only used to control the AOM, but also to trigger the boxcar integrator, as shown in Figure 1. By setting a suitable delay time in the boxcar, a TTL pulse with a duration longer than one full PZT-ramp period (i.e., >50 ms) is generated at the 'busy' output channel. This long pulse is then used as a busy-time window within which one plasma pulse is generated and absorptions are measured using cw-CRDS. In practice, the detection scheme is operated as follows:

(1) A cavity resonance generates a TTL pulse from the trigger-out terminal of the DAQ card at time t_{00}. This pulse triggers the boxcar, which has a delay time set to 75 ms. In this way, a busy-time window, beginning at t_{00} and with a 75 ms duration, is generated by the boxcar (trace d in Figure 2).
(2) The rising edge of the busy-time window triggers the multi-channel pulse generator (SRS, DG535) which provides an appropriately time-delayed pair of pulses to trigger the pulsed valve and the high voltage pulser for plasma genera-

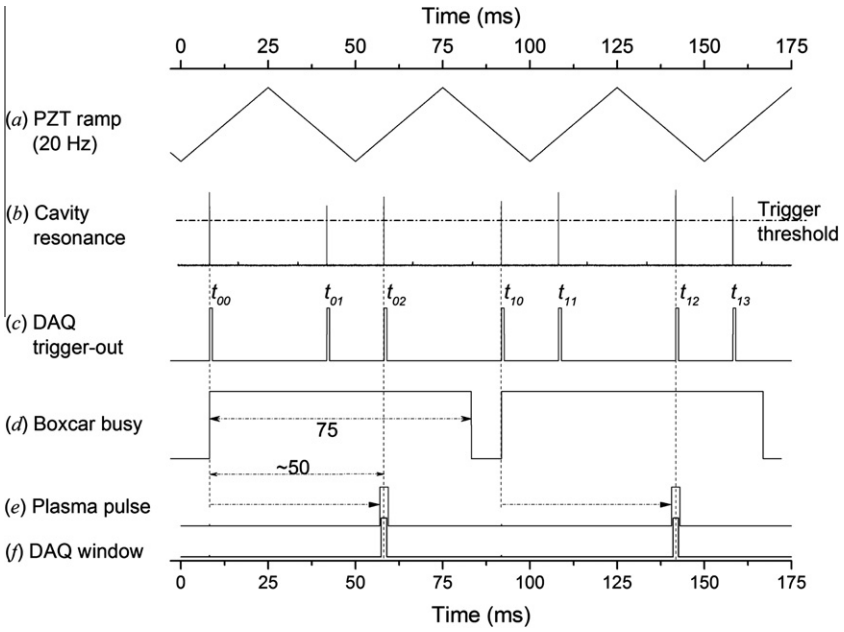

Figure 2. Timing and triggering scheme in the present experiment. For more details see the text.

tion (trace e in Figure 2). The delay times are optimized by ensuring that the center of the plasma pulse is just one PZT ramp period (i.e., 50 ms) later than t_{00}. During the 75 ms busy time, any other cavity resonances that occur (at t_{01} and t_{02}, trace b in Figure 2) will trigger the DAQ card, but not the boxcar and thus do not initiate a plasma pulse.

(3) An additional TTL pulse (~1 ms, trace f in Figure 2), synchronized with (but ~0.2 ms narrower than) the plasma pulse, is generated by the pulse generator and sent as the DAQ-time window to the second signal input channel of the DAQ card. The ring-down event that occurs in this time window, i.e., the cavity resonance at t_{02} (trace b in Figure 2), will be fitted to extract an effective ring-down time, while the events occurring at t_{00} and t_{01} (outside the time window), are not processed.

(4) After one busy-time cycle, the boxcar is triggered by the next cavity resonance at t_{10}, defining a new busy-time window for the measurement of the next plasma pulse at ~t_{12}.

In this way, each plasma pulse is activated and measured within an independent busy-time window of ~75 ms. This has the advantage that it reduces the effect of the intrinsic long time frequency drift of the OPO idler wave, as this also significantly changes the position of individual cavity resonances along the PZT-ramp. In this setting the trigger of a busy-time window may be either during a positive (e.g., at t_{00}) or negative (t_{10}) PZT-ramp, and the position of t_{00} or t_{10} with respect to the ramp will also move during a wavelength scan. It should be noted that the spacing between two busy-time windows, shown in trace d of Figure 2, depends on whether the first busy-time window covers t_{10} or not. This is determined by both the idler frequency and its drift over long time scales, and may cause the plasma repetition rate to behave in a slightly arrhythmic way. Using the experimental settings illustrated in Figure 2, approximately 10–14 plasma pulses are generated per second and more than 90% of the plasma pulses are effectively measured, i.e., coincide with a ring-down event. Non-detections mainly occur in the case that cavity resonances are too close to the turning points of the PZT-sweep. It will be shown below, that in the spectroscopic study of hydrocarbon-chain species; this issue does not significantly contribute to the noise in the final experimental spectrum.

In the detection scheme described here, the use of a boxcar integrator avoids the need for an extensive programming code for a software interface with the pulsed plasma generation, and this simplifies data acquisition. Programming and data processing are based on routine cw-CRDS technique, and only one additional procedure for the DAQ time window check is required. The present approach is different from previously applied methods [22,33,39–41] in a number of aspects: only one threshold-detection based self-trigger scheme is needed in the detection and control software; no separate programmable trigger generator (e.g., DG-535) is required; no variable trigger and timing programming is necessary; and, plasma activation is separated from the DAQ system by the boxcar, avoiding electronic noise introduced by the plasma.

The plasma absorption spectrum is subsequently recorded by measuring the ring-down time (τ) as a function of the frequency (ν) of the cw-OPO idler output. It is found that the frequency drift of the cw-OPO idler output used here may be 30 MHz over a period of ~1–2 s. This drift causes a challenge to handle; if the final spectrum is obtained in the conventional way of averaging ring-down times acquired over 1 s or longer, absorption line profiles become distorted, specifically when the absorption line widths are not very big (e.g., at the order of tens MHz). This is overcome by recording the IR frequency in parallel to the ring-down time measurement, by splitting off 1% of the idler wave – before it enters the AOM – into a wavelength meter (Bristol Instruments, 621A-IR, with a relative frequency accuracy of the order of 15 MHz). In this way, each experimental run results in an original dataset in which each data point contains both ν and τ. The original dataset is first re-sorted in the ascending order of ν, and then an average procedure on both ν and τ is performed for every fifteen data points to reduce the noise in the final spectrum. The frequency shift caused by the first order deflection of the AOM, ~80 MHz, is corrected by comparing the recorded C_2H_2 lines in the plasma jet to the available line lists in the HITRAN database [42]. The absolute frequency accuracy in our final spectrum is therefore estimated to be better than 30 MHz.

3. Results and discussion

Figure 3a shows a small part of the absorption spectrum in the 3 μm region recorded through the expanding hydrocarbon plasma. Absorption coefficients are calculated from the measured ring-down times by assuming an effective absorption path length of 3 cm in the planar plasma. Based on previous work in Refs. [30,31], most strong features in this range can be assigned to ro-vibrational transitions of the C–H asymmetric stretch modes of HC_4H and HC_6H. This is illustrated in Figure 3b where simulated spectra are shown, using previously reported molecular constants for HC_4H and HC_6H [30,31]. From the measured line intensities of HC_4H and HC_6H, the rotational temperature of these plasma jet products is estimated to be ~17 ± 3 K, comparable to values found for other transients produced in this way, but detected in optical absorption experiments (see e.g., Ref. [32]). This low temperature increases the population of the low-J'' rotational levels, and simplifies the spectral appearance of the ro-vibrational IR spectrum, also effectively increasing the detection efficiency. In Ref. [31], the analysis of the room-temperature spectrum of HC_6H is complicated by the presence of overlapping 'hot' bands, preventing the unambiguous assignment of IR features due to *para*-HC_6H, i.e., transitions from even-J'' ground state levels. Although our detection method is not mass-selective, and absorption features of other plasma products are recorded simultaneously, the much lower rotational temperature in the supersonic plasma jet makes it possible to selectively resolve IR features of HC_4H and HC_6H that have not previously been assigned. This also includes ro-vibrational transitions of *para*-HC_6H, as shown in Figure 3.

Typical full-width-at-half-maximum (FWHM) values are estimated to be ~120 MHz for HC_4H lines, and ~100 MHz for HC_6H lines. These are significantly larger than the 1 MHz bandwidth of our IR light source and due to residual Doppler broadening in the slit expansion along the cavity axis. The Doppler broadening of HC_6H in our spectrum, $(\Delta\nu/\nu) \sim 1.0 \times 10^{-7}$, is close to the value of $\sim 0.9 \times 10^{-7}$ found previously for HC_6H^+ around 600 nm [33]. The slightly larger value in the present work is likely due to the use of a larger slit width (0.3 mm), compared to 0.2 mm in Ref. [33]. A further improvement of the spectral linewidth is possible by using a narrower slit width. This however, will also decrease the signal strength as less gas is expanded.

Using the previously reported IR transition intensities for HC_4H and HC_6H nm [43,44], and the derived rotational temperature and spectral linewidth in the present work, the molecular density of ground-state HC_4H and HC_6H in our planar plasma is estimated to be of the order of $\sim 10^{11}$–10^{12} molecules/cm^3, comparable to the value found recently for C_6H using cavity enhanced plasma self-absorption spectroscopy nm [35]. The density ratio $N(HC_4H)/N(HC_6H)$ in the hydrocarbon plasma is found to be ~2.5 ± 0.5, indicating that also longer and more complex carbon-chain species should be detectable with the spectroscopic scheme presented here. Evidence for this is also visible in Figure 3a. All of the weaker and unassigned features here are reproduced in independent measurements and stand for unassigned transitions.

The interpretation of the weak features is consistent with the noise level in the present experiment. To evaluate the detection sensitivity of our method, an additional measurement is performed without plasma, i.e., under conditions in which only absorption features due to the precursor gas are expected. This is necessary because of a broad weak absorption $\sim(3–5) \times 10^{-6}$ cm^{-1} found in our experimental spectra (reflected by a non-zero spectral 'baseline' as shown in Figure 3). The recorded spectrum is shown in Figure 4a (lower trace) and compared to the absorption spectrum with discharge on (upper trace). Without discharge, a single strong absorption line due to C_2H_2 is observed and the baseline is flat. An expanded view of the baseline in Figure 4b indicates a detection sensitivity of the order of 2.0×10^{-7} cm^{-1}, supporting the claim that the present setup indeed has much potential to record IR features of transient species through an expanding hydrocarbon plasma. It should be noted that the actual noise level in the plasma

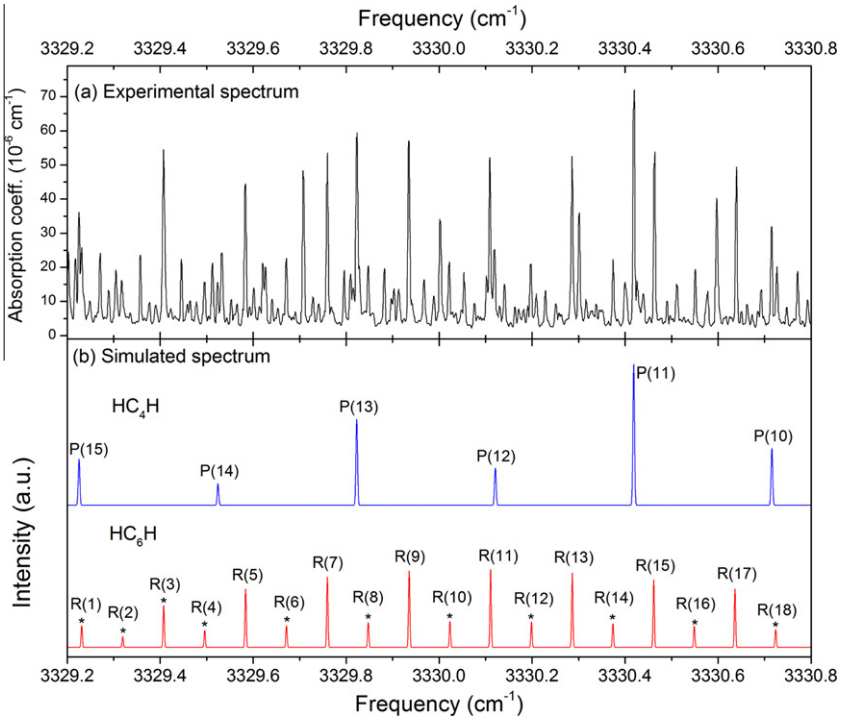

Figure 3. A portion of the experimental spectrum (panel a) recorded through a hydrocarbon plasma expansion by discharging a C_2H_2/He/Ar gas mixture. Features due to ro-vibrational transitions of HC_4H and HC_6H are indicated by the simulated spectrum in panel (b). Spectral linewidths of 120 MHz for HC_4H and 100 MHz for HC_6H, and a rotational temperature of 17 K are used in the simulation. Lines marked by asterisks in the simulated HC_6H spectrum are features that were not observed in Ref. [31].

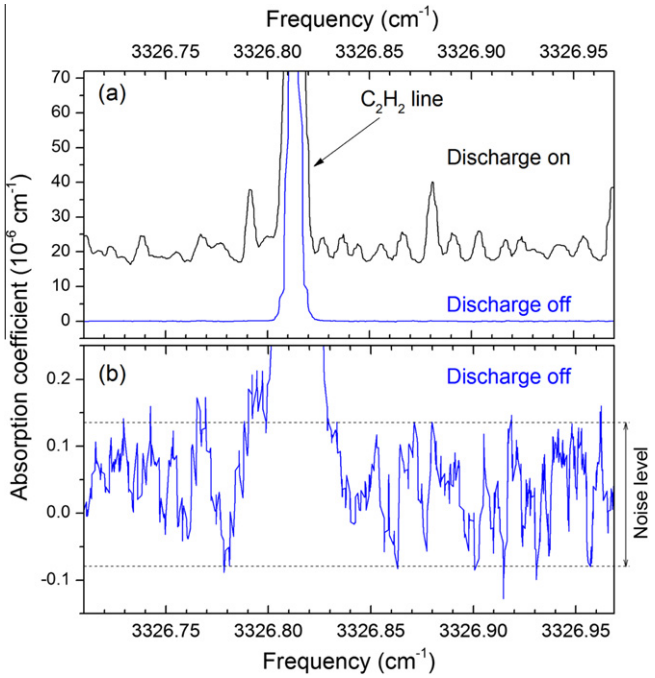

Figure 4. (a) The experimental spectra recorded with discharge on (upper trace, offset by 15×10^{-6} cm^{-1}) and off (lower trace); (b) an expanded view of the baseline from the experimental spectrum with discharge off. The noise level in the present cw-CRDS experiment is indicated in panel (b).

measurement may be larger than this number because of the variations in the measurements due to the timing jitter and shot-to-shot fluctuations of the pulsed plasma. This increases the noise level proportionally to the absolute absorbance and as discussed in the Supplementary material of Ref. [22], this affects the measured line profiles. Under the experimental conditions described in Section 2, this variation is ~20%, which is significantly less than found in Ref. [22], and moreover, this value can be further reduced to ~5% by an averaging procedure. This allows us to analyze the observed peaks including most of the weak features with Gaussian line shapes. Meanwhile, the increase of the noise level in weak absorption regions (with typical absorbances smaller than 1.0×10^{-5} cm^{-1}) is estimated to be $\sim 5.0 \times 10^{-7}$ cm^{-1} or even smaller, and therefore, this will not be case limiting here.

Finally, we also have measured spectra in the 3305–3341 cm^{-1} region, which is characteristic of the –(C≡C)–H stretch vibration of both HC_4H and HC_6H, as reported in Refs. [30,31]. Although the experiment is performed for supersonic jet conditions, in total more than 2000 lines are recorded, and a preliminary analysis shows that more than 600 lines can be assigned to vibrational hot bands (including several new weak bands) of di- and tri-acetylene. Other features, particularly weak ones, are likely due to other long hydrocarbon chains and new vibrational hot band transitions of di- and tri-acetylene involving heavy perturbations. A full analysis of the spectrum in the 3 μm region, including hot bands, will be published separately.

The method demonstrated here is an extension of previous laboratory microwave and optical work on carbon-chain species, and is generally applicable for high-resolution infrared investigations of molecular transients. Recent developments of the cw-OPO technique nm [45] allow applications of this method to be extended to wavelengths as long as 8 μm. The setup described here has astrochemical potential. As has been found in our previous optical work for C_6H nm [34], carbon-chains populated in low-lying vibrational states can be produced in sufficient quantities, using the source described in Section 2.1. In general, transitions involving the characteristic bending vibrations of long chains are in the millimeter/THz region and of direct astronomical importance. Using the method presented here, accurate ro-vibrational energies can be studied indirectly by measuring vibrational difference or hot band transitions of vibrationally excited species in the mid-IR region. These mid-IR data allow for the accurate calculation of spectroscopic parameters which can be further used to predict molecular transitions in the millimeter/THz region. This information is needed for the most recent class of astronomical flagship facilities: HIFI/Herschel, SOFIA and ALMA, in order to discriminate the unidentified features in the observed spectrum that covers thousands of lines.

Acknowledgements

This work has been realized with financial support of SRON and a NWO-VICI grant (Linnartz). We acknowledge the experimental assistance of Kirstin Doney (Leiden).

References

[1] M.C. McCarthy, P. Thaddeus, Chem. Soc. Rev. 30 (2001) 177.
[2] H.S.P. Müller, F. Schlöder, J. Stutzki, G. Winnewisser, J. Mol. Struct. 742 (2005) 215.
[3] M.B. Bell, P.A. Feldman, M.J. Travers, M.C. McCarthy, C.A. Gottlieb, P. Thaddeus, Astrophys. J. 483 (1997) L61.
[4] C.A. Gottlieb, A.J. Apponi, M.C. McCarthy, P. Thaddeus, H. Linnartz, J. Chem. Phys. 113 (2000) 1910.
[5] M.C. McCarthy, C.A. Gottlieb, H. Gupta, P. Thaddeus, Astrophys. J. 652 (2006) L141.
[6] S. Brunken, H. Gupta, C.A. Gottlieb, M.C. McCarthy, P. Thaddeus, Astrophys. J. 664 (2007) L43.
[7] K.H. Hinkle, J.J. Keady, P.F. Bernath, Science 241 (1988) 1319.
[8] P.F. Bernath, K.H. Hinkle, J.J. Keady, Science 244 (1989) 562.
[9] J.R. Heath, R.A. Sheeks, A.L. Cooksy, R.J. Saykally, Science 249 (1990) 895.
[10] T.F. Giesen, A. van Orden, H.J. Hwang, R.S. Fellers, R.A. Provencal, R.J. Saykally, Science 265 (1994) 756.
[11] A. van Orden, R.J. Saykally, Chem. Rev. 98 (1998) 2313.
[12] J. Cernicharo, A.M. Heras, A.G.G.M. Tielens, J.R. Pardo, F. Herpin, M. Guélin, L.B.F.M. Waters, Astrophys. J. 546 (2001) L123.
[13] J.P. Fonfría, J. Cernicharo, M.J. Richter, J.H. Lacy, Astrophys. J. 728 (2011) 43.
[14] A.E. Douglas, Nature 269 (1977) 130.
[15] J. Fulara, D. Lessen, P. Freivogel, J.P. Maier, Nature 366 (1993) 439.
[16] E.B. Jochnowitz, J.P. Maier, Annu. Rev. Phys. Chem. 59 (2008) 519.
[17] R. Nagarajan, J.P. Maier, Int. Rev. Phys. Chem. 29 (2010) 521.
[18] S. Albert, K.K. Albert, M. Quack, in: M. Quack, F. Merkt (Eds.), Handbook of High Resolution Spectroscopy, John Wiley & Sons, 2011, p. 965.
[19] M. Snels, V. Horká-Zelenká, H. Hollenstein, M. Quack, in: M. Quack, F. Merkt (Eds.), Handbook of High Resolution Spectroscopy, John Wiley & Sons, 2011, p. 1021.
[20] M.W. Sigrist, in: M. Quack, F. Merkt (Eds.), Handbook of High Resolution Spectroscopy, John Wiley & Sons, 2011, p. 1129.
[21] H. Verbraak, A.K.Y. Ngai, S.T. Persijn, F.J.M. Harren, H. Linnartz, Chem. Phys. Lett. 442 (2007) 145.
[22] B.A. Tom, A.A. Mills, M.B. Wiczer, K.N. Crabtree, B.J. McCall, J. Chem. Phys. 132 (2010) 081103.
[23] H. Kreckel et al., Phys. Rev. A 82 (2010) 042715.
[24] B.E. Brumfield, J.T. Stewart, S.L.W. Weaver, M.D. Escarra, S.S. Howard, C.F. Gmachl, B.J. McCall, Rev. Sci. Instrum. 81 (2010) 063102.
[25] M.W. Porambo, B.M. Siller, J.M. Pearson, B.J. McCall, Opt. Lett. 37 (2012) 4422.
[26] K.N. Crabtree, J.N. Hodges, B.M. Siller, A.J. Perry, J.E. Kelly, P.A. Jenkins II, B.J. McCall, Chem. Phys. Lett. 551 (2012) 1.
[27] P. Neubauer-Guenther, T.F. Giesen, U. Berndt, G. Fuchs, G. Winnewisser, Spectrochim. Acta A 59 (2003) 431.
[28] M.J. Krieg, A. Kleemann, I. Gottbehüt, S. Thorwirth, T.F. Giesen, S. Schlemmer, Rev. Sci. Instrum. 82 (2011) 063105.
[29] S. Thorwirth et al., J. Mol. Spectrosc. 270 (2011) 75.
[30] G. Guelachvili, A.M. Craig, D.A. Ramsay, J. Mol. Spectrosc. 105 (1984) 156.
[31] K. Matsumura, K. Kawaguchi, D. McNaughton, D.N. Bruget, J. Mol. Spectrosc. 158 (1993) 489.
[32] T. Motylewski, H. Linnartz, Rev. Sci. Instrum. 70 (1999) 1305.
[33] P. Birza, T. Motylewski, D. Khoroshev, A. Chirocolava, H. Linnartz, J.P. Maier, Chem. Phys. 283 (2002) 119.
[34] D. Zhao, M.A. Haddad, H. Linnartz, W. Ubachs, J. Chem. Phys. 135 (2011) 044307.
[35] A. Walsh, D. Zhao, H. Linnartz, Appl. Phys. Lett. 101 (2012) 09111.
[36] A. Walsh, D. Zhao, H. Linnartz, J. Phys. Chem. A (2013), http://dx.doi.org/10.1021/jp310392n.
[37] Y. He, M. Hippler, M. Quack, Chem. Phys. Lett. 289 (1998) 527.
[38] D. Halmer, G. von Basum, P. Hering, M. Murtz, Rev. Sci. Instrum. 75 (2004) 2187.

[39] M. Hippler, M. Quack, Chem. Phys. Lett. 314 (1999) 273.
[40] P. Birza, D. Khoroshev, A. Chirokolava, T. Motylewski, J.P. Maier, Chem. Phys. Lett. 382 (2003) 245.
[41] W.S. Tam, I. Leonov, Y. Xu, Rev. Sci. Instrum. 77 (2006) 063117.
[42] L.S. Rothman et al., J. Quant. Spectrosc. Radiat. Transfer 110 (2009) 533.
[43] M. Khlifi, P. Paillous, C. Delpech, M. Nishio, P. Bruston, F. Raulin, J. Mol. Spectrosc. 174 (1995) 116.
[44] F. Shindo, Y. Benilan, J.C. Guillemin, P. Chaquin, A. Jolly, F. Raulin, Planet. Space Sci. 51 (2003) 9.
[45] S. Vasilyev et al., Opt. Lett. 33 (2008) 1413.